Published in final edited form as:
Traffic. 2012 May ; 13(5): 715–726. doi:10.1111/j.1600-0854.2012.01337.x.

The Formation and Stability of DC-SIGN Microdomains Require its Extracellular Moiety

Ping Liu[‡], **Xiang Wang**[§], **Michelle S. Itano**[‡], **Aaron K. Neumann**[‡], **Ken Jacobson**[‡,¶,1,2], and **Nancy L. Thompson**[§,1,2]

[‡]Department of Cell and Developmental Biology, University of North Carolina at Chapel Hill, Chapel Hill, NC 27599

[§]Department of Chemistry, University of North Carolina at Chapel Hill, Chapel Hill, NC 27599

[¶]Lineberger Comprehensive Cancer Center, University of North Carolina at Chapel Hill, Chapel Hill, NC 27599

Abstract

DC-SIGN (Dendritic cell-specific ICAM-3-grabbing non-integrin) is a Ca^{2+}-dependent transmembrane lectin that binds a large variety of pathogens and facilitates their uptake for subsequent antigen presentation. This receptor is present in cell surface microdomains, but factors involved in microdomain formation and their exceptional stability are not clear. To determine which domain/motif of DC-SIGN facilitates its presence in microdomains, we studied mutations at key locations including truncation of the cytoplasmic tail, and ectodomain mutations that resulted in removal of the N-linked glycosylation site, the tandem repeats and the carbohydrate recognition domain (CRD) as well as modification of the calcium sites in the CRD required for carbohydrate binding. Confocal imaging and FRAP measurements showed that the cytoplasmic domain and N-linked glycosylation site do not affect the ability of DC-SIGN to form stable microdomains. However, truncation of the CRD results in complete loss of visible microdomains and subsequent lateral diffusion of the mutants. Apart from cell adhesions, membrane domains are thought to be localized primarily via the cytoskeleton. By contrast, we propose that interactions between the CRD of DC-SIGN and the extracellular matrix and/or cis interactions with transmembrane scaffolding protein(s) play an essential role in organizing these microdomains.

Keywords

CD209; membrane microdomain; live cell fluorescence imaging; pathogen uptake; antigen presentation; fluorescence recovery after photobleaching; membrane protein dynamics; extracellular matrix

Introduction

Dendritic cell-specific ICAM-3-grabbing non-integrin (DC-SIGN) is a pattern recognition receptor which is expressed by monocyte-derived dendritic cells (DCs). It binds to mannose and fucose structures on the surface of a broad range of pathogens, including viruses, bacteria and parasites and plays a crucial role in stimulation of diverse immune responses (1). This receptor is of fundamental importance for understanding the molecular mechanism underlying pathogen recognition by DCs. This lectin captures pathogens through

[2]To whom correspondence should be addressed: Ken Jacobson, frap@med.unc.edu or Nancy L. Thompson, nlt@unc.edu.
[1]Ken Jacobson and Nancy L. Thompson contributed equally to this work.

interactions between its carbohydrate recognition domain (CRD) and carbohydrates on the surface of pathogens. The monomeric CRD exhibits low binding affinity to high mannose carbohydrates, while tetramerization of DC-SIGN, facilitated by the tandem repeats in the extracellular region, greatly enhances DC-SIGN's binding affinity (2). Moreover, DC-SIGN forms clusters or microdomains on the DC plasma membrane (3–5) that act as docking sites for various pathogens. Clustering of DC-SIGN probably not only increases its avidity to carbohydrate ligands, but also modulates its specificity by favoring carbohydrates with a certain density and spacing (6). We reported that cell lines ectopically expressing DC-SIGN also form similar, discrete surface microdomains that range in size from the diffraction limit to over 1 μm in diameter (5). These microdomains are extremely stable on the cell membrane in terms of the lack of lateral movement of DC-SIGN within the microdomains as well as the lack of exchange of the lectin with any pool in the surrounding membrane, although occasionally the microdomains will exhibit rapid retrograde transport prior to internalization (5, 7). Moreover, microdomain formation and stability do not appear to require the cytoplasmic domain of DC-SIGN (7).

At this juncture, the molecular origins of the formation and unexpected stability of DC-SIGN microdomains remain a mystery. Because DC-SIGN forms microdomains when ectopically expressed in a variety of cells (5), a mutational strategy offers one approach to unraveling this mystery. We generated a collection of mutants in which the cytoplasmic domain was deleted, the N-linked glycosylation site was not operative, the tandem repeats were deleted, or the CRD was deleted. We then evaluated domain formation visually with fluorescence microscopy and measured the size of the microdomains, if they existed; the stability of the microdomains was evaluated by fluorescence recovery after photobleaching (FRAP) since we knew that wild-type (wt) DC-SIGN microdomains are extraordinarily stable, exhibiting almost no recovery (5, 7). Our results indicate that the tandem repeats and CRD play crucial roles in DC-SIGN microdomain formation and stability, the latter either by directly interacting with extracellular matrix components and/or via *cis* interactions with a transmembrane adaptor protein(s). This result has significance beyond DC biology since there is little precedence for extracellular stabilization of membrane domains apart from cell-cell and cell substratum adhesions where both extracellular and cytoskeletal factors are involved.

RESULTS

Mutations of DC-SIGN

Different regions of DC-SIGN were mutated to investigate which domain/motif(s) of DC-SIGN facilitate microdomain formation and stability. Four types of mutations were produced (Figure 1A): truncation of the cytoplasmic region (the first 37 amino acids at the N-terminus were removed, denoted as DC-SIGN-Δ37); a point mutation of the N-linked glycosylation site (denoted as DC-SIGN-N80Q) that prevents glycosylation at this site; deletion of the seven and one half tandem repeats in the extracellular region (denoted as DC-SIGN-ΔRepeats); and truncation of the CRD (denoted as DC-SIGN-ΔCRD). An AU1 antigenic tag was introduced at the C-terminus of the ΔCRD mutation, so that the truncated receptor could be directly detected by a fluorescent dye - conjugated monoclonal antibody (mAb). In addition, EGFP conjugated forms of wt and these mutations were generated. Figure 1B shows the Western blots obtained from cells expressing wt DC-SIGN or its mutants. Figures 2, 3, 4, 5, and 6 present the images, FRAP and microdomain sizing results characterizing these mutant DC-SIGN molecules; the results are summarized in Table 1.

Neither the cytoplasmic tail of DC-SIGN nor its N-linked glycosylation site is required for stable cell surface microdomains

We previously found that microdomains of DC-SIGN on cell surfaces are extremely stable in terms of location and diffusion of the receptor within the microdomain, as well as exchange between the microdomain and surround (5, 7). One possibility is that the cytoplasmic tail of DC-SIGN may directly associate with cytoskeletal structures, such as actin filaments, that stabilize the microdomains on the surface and immobilize DC-SIGN within the microdomains. If this hypothesis is correct, truncation of the cytoplasmic region would eliminate such interactions and release immobile DC-SIGN. However, two cytoplasmic truncation mutants, DC-SIGN-Δ20 and DC-SIGN-Δ35, still form stable, discrete microdomains on cell membranes (7). To confirm and extend these earlier measurements, we made the DC-SIGN-Δ37 construct (Figure 1A), which further removed residue Cys^{37}, the single cysteine that locates outside the CRD. As shown in Figure 2 C and D, DC-SIGN-Δ37 (mAb-labeled) and GFP-DC-SIGN-Δ37 still formed discrete microdomains on cell membranes, indicating that residue Cys^{37} is not directly involved in the membrane microdomain formation.

Next, we carried out FRAP measurements on cells expressing DC-SIGN-Δ37 (visualized with a dye-conjugated mAb; i.e., AlexaFluor 488 conjugated 120507 mAb) or GFP-DC-SIGN-Δ37 to examine whether these mutants could diffuse within the microdomain and exchange with the surround. As shown in Figure 3 C and D, little recovery was observed after photobleaching, indicating that the microdomains formed by DC-SIGN-Δ37 or GFP-DC-SIGN-Δ37 are stable and do not exchange appreciably with surrounding molecules of the same type, similar to those formed by wt DC-SIGN (Figure 3 A and B) (5, 7). Therefore, truncation of the cytoplasmic region of DC-SIGN does not significantly affect either microdomain formation or stability.

One potential function of residue Cys^{37}, in the cytoplasmic tail of DC-SIGN near the inner leaflet of the plasma membrane, is that it may be a palmitoylation site, similar to the cysteine residues in the juxtamembrane region of β_1-adrenergic receptors (8). Like the palmitoylation of the cysteine residue in the plasma membrane targeting sequence of the retinitis pigmentosa protein RP2 (9), palmitoylation of the cysteine residue in the juxtamembrane region may help to stabilize the receptor in the plasma membrane, and may also function in concentrating the receptors in certain membrane regions that are rich in saturated lipids (10). Indeed, we observed a colocalization of wt DC-SIGN with a membrane fluorescent protein probe, PMT-mRFP (*p*lasma *m*embrane *t*arget mRFP, which contains a myristoylation site and a potential palmitoylation site (9, 11)), when coexpressing wt DC-SIGN and PMT-mRFP in NIH3T3 cells (Figure S1, Supporting information), consistent with previous reports of 'raft' localization of DC-SIGN (3, 12). However, since DC-SIGN-Δ20, DC-SIGN-Δ35 and DC-SIGN-Δ37 are all able to form stable surface microdomains, it is unlikely that the microdomains are maintained by interactions involving potential palmitoylation of DC-SIGN and inner leaflet lipids.

The N-linked consensus sequence is Asn-X-Ser/Thr, in which X can be any amino acid except proline. DC-SIGN contains a potential N-linked glycosylation site, residues Asn^{80}-Leu^{81}-Thr^{82} (13). Extracellular secreted galectins bind to exposed sugar residues forming putative galectin-glycoprotein lattices on the cell surface (14). Thus, DC-SIGN could be cross-linked by galectins through the glycosylated Asn^{80}, which might be a mechanism for DC-SIGN microdomain formation. To test this hypothesis, we switched residue Asn^{80} to a Gln by site-directed mutagenesis. As shown in Figure 2 E and F, both DC-SIGN-N80Q and GFP-DC-SIGN-N80Q still form distinct surface microdomains and little recovery was observed after photobleaching such microdomains (Figure 3 E and F, respectively).

Therefore, our results imply that N-glycosylation on residue Asn^{80} is not a primary factor involved in DC-SIGN microdomain formation or stability.

Note that the total numbers of microdomains in Figures 2 B, D, and F (the GFP-containing constructs) are less than the numbers of microdomains formed by the corresponding non-GFP containing constructs. This result may be caused by the proximity of GFP to the inner leaflet, which could affect a step and/or steps during initial synthesis, plasma membrane delivery, and/or microdomain formation. However, the average number of microdomains on cells expressing GFP-DC-SIGN-N80Q is approximately equivalent to cells expressing GFP-DC-SIGN (Table 1).

To examine whether there is a size difference between the microdomains formed by wt DC-SIGN and the microdomains formed by the various mutants, we measured the size distributions of these microdomains. Figure 4 A–F gives the size distribution of microdomains formed by each DC-SIGN construct. In general, the microdomains formed by wt DC-SIGN are smaller and more uniform in dimension, while the microdomains formed by the DC-SIGN-Δ37 and N80Q mutations are larger and exhibit a larger size range (Figure 4 G and Table 1). This result suggests that the cytoplasmic tail and the glycosylation site play a role in fine-tuning the microdomain structure. Indeed, as reported by Serrano-Gómez *et al.*, the glycosylation site mutation (N80Q) resulted in an increased proportion of high order oligomers compared to wt DC-SIGN (15). On the other hand, the three EGFP fusions all exhibit a larger microdomain size compared to the microdomains formed by their corresponding non-fluorescent mutant proteins; it is possible that the cytoplasmic tail might also negatively affect oligomer formation and that an EGFP tagged to the terminus of the cytoplasmic tail may reduce such an effect. Nonetheless, as both the cytoplasmic tail truncation and glycosylation site mutation of DC-SIGN form stable, discrete microdomains, we conclude that the neither the cytoplasmic tail nor N-linked glycosylation provides the major driving force for surface microdomain formation.

Deletion of the tandem repeats results in a combination of lateral diffusion of DC-SIGN and some microdomain formation on cell surfaces

In contrast to the cytoplasmic truncation and N-linked glycosylation site mutation, deletion of the tandem repeats of DC-SIGN results in loss of stable microdomains. Figure 5 A shows that diffuse membrane fluorescence was observed on cells expressing either the GFP-DC-SIGN-Δrepeats (A-1) or the DC-SIGN-Δrepeats labeled with 120507 mAbs conjugated to AlexaFluor 488 (A-2). FRAP measurements on these cells show that after deletion of the tandem repeats the majority of the receptors are mobile on the membrane (Figure 5 C and D). The mobile fractions, P_∞, for GFP-DC-SIGN-Δrepeats and mAb labeled DC-SIGN-Δrepeats are 78 ± 5% (±SEM, N=13) and 67 ± 10% (±SEM, N=10), respectively. The corresponding diffusion coefficients, D, for GFP-DC-SIGN-Δrepeats and DC-SIGN-Δrepeats labeled by Alexa488-conjugated mAb are 0.12 ± 0.02 $\mu m^2/s$ (±SEM, N=13) and 0.08 ± 0.03 $\mu m^2/s$ (±SEM, N=10), respectively. A fraction of cells expressing either GFP-DC-SIGN-Δrepeats or DC-SIGN-Δrepeats (mAb-labeled), particularly at high expression levels, showed some punctate labeling together with diffuse membrane fluorescence. Figure 5 B gives an example of a cell expressing GFP-DC-SIGN-Δrepeats, which showed bright microdomain-like spots (Figure 5 B-1; red arrow) as well as diffuse membrane fluorescence (Figure 5 B-1; yellow arrow). Such ‘microdomains’ differ markedly from the stable domains formed by wt DC-SIGN because 1) the ‘domains’ are dynamic and can often move from one position to other positions on the membrane, as observed by time-lapse confocal imaging (data not shown); and 2) DC-SIGN within these ‘domains’ is able to exchange with DC-SIGN in the surrounding membrane, as shown by the recovery after photobleaching (Figure 5 E and F). The recovery curves of these ‘dynamic microdomains’ are often non-monotonic, which might be due to membrane fluctuation or slight domain movement during the

recovery phase. In addition, the recovery rate is slower compared to that in the surrounding membrane, suggesting that transient binding to anchoring structures within the microdomain and/or a partially permeable barrier surrounding the microdomain may be occurring (16, 17).

The observation of diffuse membrane fluorescence and 'dynamic microdomains' on cells expressing the tandem repeats deletion mutation is different from the observation on cells expressing the CRD truncation mutants, which only show homogenous, diffuse membrane fluorescence, as we discuss in the next section. One possibility is that after removal of the tandem repeats, DC-SIGN partially retains its biological function; i.e., the CRD could still bind to ligands that now weakly promote the formation of much less stable microdomains.

Truncation of the CRD results in complete loss of visible microdomains on cell surfaces

Removal of the CRD of DC-SIGN results in a complete loss of visible microdomains on the cell surface. Figure 6 A shows that cells expressing GFP-DC-SIGN-ΔCRD (Figure 6 A-1 and A-3) and cells expressing DC-SIGN-ΔCRD labeled by FITC-conjugated mAb against the AU1 tag (Figure 6 A-2 and A-4) exhibit diffuse membrane fluorescence, but no distinct surface microdomains. Furthermore, recovery was observed after photobleaching a circular membrane area (Figure 6 B and C), indicating that CRD truncation mutants are laterally mobile in the plasma membrane. The average mobile percentage P_∞ for GFP-DC-SIGN-ΔCRD is 95 ± 4 % (±SEM, N=15), and for DC-SIGN-ΔCRD labeled by FITC-conjugated mAb the P_∞ value is 73 ± 7% (±SEM, N=11). The diffusion coefficients, D, for GFP-DC-SIGN-ΔCRD and DC-SIGN-ΔCRD labeled by FITC-conjugated mAb are 0.18 ± 0.02 $\mu m^2/s$ (±SEM, N=15) and 0.02 ± 0.01$\mu m^2/s$ (±SEM, N=11), respectively. Nonetheless, both the mAb-labeled and the GFP-fused CRD truncation mutants showed diffuse and homogenous membrane fluorescence, indicating that DC-SIGN loses both its ability to form microdomains as well as its immobilization on the membrane without the CRD. This behavior was independent of expression level (not shown). These experiments form, in a sense, a positive control for the cytoplasmic truncation and N-linked glycosylation site mutants in which microdomains were formed and very little fluorescence recovery after photobleaching was observed.

Lastly, preliminary data show that mutating one of the seven residues involved in calcium coordination that are key to saccharide binding in the CRD also shows no evidence for microdomains and that the mutant exhibits nearly complete recovery (Figure S2, Supporting information); this result further implicates saccharide binding in the CRD as the primary source of DC-SIGN stabilization in microdomains.

DISCUSSION

Because the molecular origins of the formation and unexpected stability of DC-SIGN microdomains were unknown, we pursued a mutational approach to investigate these intriguing issues. These mutations were aimed to disrupt the cytoplasmic and extracellular regions of DC-SIGN. This strategy is at least partially justified by the observation that DC-SIGN becomes laterally mobile in giant plasma membrane vesicles formed from cells expressing the receptor as judged by its collection at the interface between two closely apposed vesicles (Levental I., Liu P., Thompson N. L., Simons K. and Jacobson K., unpublished results); such vesicles would be expected to have significantly depleted associated cytoskeletal and pericellular matrix structures (18, 19). Moreover, ectopically expressed DC-SIGN forms domains that are similar to those found in DCs (5, 7). It should be noted that our analysis was performed using widefield microscopy methods. However, as shown by super-resolution Blink Microscopy and electron microscopy, domains that appear

contiguous in widefield microscopy are most likely composed of arrays of nanodomains of dimensions < 100 nm (4, Itano et al., unpublished).

We extended our previous finding (7) that DC-SIGN cell surface microdomain formation does not require its cytoplasmic tail. The conventional notion would be that the cytoplasmic tail of DC-SIGN could associate with cytoskeleton structures proximate to the membrane and that this would confer the extreme stability of wt DC-SIGN microdomains. Indeed, Gringhuis *et al.* reported that the cytoplasmic domain of DC-SIGN constitutively associates with scaffold proteins LSP1 (Leukocyte-specific protein 1), KSR1 (kinase suppressor of Ras1) and CNK (connector enhancer of KSR); moreover, LSP1 is an actin-binding protein (20). Therefore one might expect that DC-SIGN could be immobilized through a linkage from its cytoplasmic tail to the membrane apposed cytoskeleton via scaffold proteins. However, the three cytoplasmic mutants (DC-SIGN-Δ20, DC-SIGN-Δ35 and DC-SIGN-Δ37) tested in this and our previous work (7) all form stable microdomains in the plasma membrane, indicating that *direct* association between the cytoplasmic domain of DC-SIGN and the membrane-apposed cytoskeleton is not the major initial driving force for membrane microdomain formation and stability. This conclusion does not preclude *cis* associations with other transmembrane proteins that are themselves linked to the membrane apposed cytoskeleton (Figure 7), although administration of two different actin cytoskeletal disrupting drugs, cytochalasin D and latrunculin, did not affect microdomain formation (Supplemental Figure S3). Whether or not the cytoskeleton is indirectly involved in microdomain stability, the cytoplasmic tail is certainly involved via adaptors and scaffolding proteins in various downstream signaling networks in response to pathogen binding (20, 21).

The N-linked glycosylation site is not required for microdomain formation and stability. Using biochemical assays, the N80Q mutation has been reported to form higher order oligomers other than monomers or tetramers (15) which may contribute to the fact that the N80Q mutant forms larger sized microdomains. Moreover, putative galectin-mediated lattice formation (14) employing this glycosylation site does not appear to occur.

In terms of proposing a mechanism for the formation and unusual stability of DC-SIGN microdomains, the most intriguing observations are that the tandem repeats deletion and CRD truncation resulted in the loss of stable microdomains. The tandem repeats region is proposed to facilitate tetramerization of DC-SIGN by forming coiled-coil α-helices (13), and biochemical assays have shown that after deletion of the tandem repeats DC-SIGN is not able to tetramerize, and instead exists mainly as monomers (15, 22). It has also been suggested that the tandem repeats and the CRD fold independently, and that the CRD is flexibly linked to the tandem repeats (22). Therefore, it is feasible that after removal of either the tandem repeats or the CRD, the remaining sequence could still fold properly.

We observed a complete loss of microdomain formation in cells expressing the CRD truncation mutants, and both DC-SIGN-ΔCRD (mAb-labeled) and GFP-DC-SIGN-ΔCRD are able to laterally diffuse on the plasma membrane. This observation indicates that DC-SIGN with the tandem repeats region alone, but lacking the CRD, is not able to form stable microdomains although it could still tetramerize as reported by Yu *et al.* (23). By contrast, after deleting the tandem repeats, the receptor was still able to form some dynamic microdomains on cell surfaces especially at high expression levels. This observation indicates that the CRD has the capability to promote clustering although such clusters lack the extreme stability of wt DC-SIGN microdomains. These results suggest the hypothesis that the CRD plays a major role in microdomain formation and the tandem repeats co-operate and stabilize the microdomains.

Indeed, our results lead to the proposal of a model for the origin of DC-SIGN microdomain stability. Microdomain stability may be primarily facilitated by the CRD of DC-SIGN directly binding to polysaccharides (e.g., glycosaminoglycans or glycosyl moieties of extracellular matrix (ECM) proteins) in the ECM (Figure 7 A), or, by DC-SIGN directly binding to transmembrane proteoglycans that link to the ECM (Figure 7 B). It is also possible that glycosylated transmembrane adaptor proteins (TRAPs) (24), that are directly or indirectly linked to the membrane apposed cytoskeleton and have *cis* interactions with DC-SIGN, serve to stabilize these microdomains (Figure 7 C). For example, the CRD of DC-SIGN could recognize transmembrane proteoglycans (25) that are linked to the cytoskeleton thus serving to stabilize microdomains. Such proteins could also serve as pathogen co-receptors enabling differentiation of downstream pathways in response to the variety of pathogens that DC-SIGN binds (20, 21, 26). Although not depicted, it is also possible that secreted galectins (14) could mediate formation and stabilization of microdomains via binding smaller saccharide ligands bound to the CRD and glycosyl moieties of ECM components and/or transmembrane proteoglycans and TRAPs.

The tandem repeats region in this hypothesis would play two important roles: first, it is involved in oligomerizing/tetramerizing the receptors (15, 23) which acts to increase the avidity by providing four CRDs in close proximity; second, the tandem repeats project the CRD toward potential ligands within the ECM. Loss of either or both of these functions, for the tandem repeats deletion mutant, could be the explanation for both the lower number of microdomains and their reduced stability. Finally, the importance of carbohydrate recognition in microdomain stability is also seen by the fact that when DCs are incubated with 0.2 M lactose, microdomains are seen to become more diffuse and less organized (Supplemental Figure S4).

Additional significance derives from the fact that apart from cell-cell junctions (27) including the neuromuscular junction (28) and cell-substratum adhesions (29), where both extracellular and cytoskeletal factors come into play, there is relatively little precedence for an important role for extracellular stabilization of membrane domains on free cell surfaces; indeed, we may expect other examples of this motif to appear in other biological contexts.

A plausible working hypothesis relating microdomain structure to function emerges that is similar to the SIGLEC hypothesis for lymphoid cells (32, 33): Pathogens with closely spaced high mannose structures on their surfaces (34) compete with the binding of the CRD to polysaccharides in the ECM, to activate the receptors and initiate downstream signaling cascades leading to pathogen internalization. If this hypothesis were correct, it would suggest that both the mobility of DC-SIGN within microdomains (5–7) and the nanostructure of the microdomains (4, Itano et al., unpublished) may be altered upon encountering pathogens to facilitate optimal binding and subsequent internalization and processing.

Materials and Methods

Plasmids

The construction of pEGFP-C1/DC-SIGN, a plasmid encoding human DC-SIGN in a modified pEGFP-C1 (Clontech, Palo Alto, CA) vector (in which the EGFP gene was removed) was described elsewhere (7). The pMX/GFP-DC-SIGN plasmid was kindly provided by Dr. Dan Littman, New York University and Howard Hughes Medical Institute, New York, NY. The plasmid was then digested with *BamH*I and *Not*I, and GFP-DC-SIGN fragment was inserted into pEGFP-N1 vector digested with *BamH*I and *Not*I, to generate pEGFP-N1/GFP-DC-SIGN. We previously reported that two cytoplasmic truncations of DC-SIGN, DC-SIGN-Δ20 and DC-SIGN-Δ35 (in which the first 20 or 35 amino acids from

the N-terminus were removed) showed no visible effect on membrane microdomain formation (7). In this study, we further truncated the first 37 aa, i.e. DC-SIGN-Δ37, to examine whether residue Cys^{37} is involved in the cell surface microdomain formation. The following two oligonucleotide primers with an *Age*I or *Not*I site (underlined) were used to generate the DC-SIGN-Δ37 fragment, using pEGFP-C1/DC-SIGN as the template: 5'-CCACCGGTCGCCACCATGCTTGGCCATGGTCCCCTGGTG (primer A) and 5'-TAAAGCGGCCGCTCTACGCAGGAGGGGGGTTTGG (primer B). The resulting PCR product was digested and inserted into pEGFP-N1 vector (Clontech) by replacing the EGFP sequence through *Age*I and *Not*I sites. The two N-linked glycosylation site mutation constructs, i.e. DC-SIGN-N80Q and GFP-DC-SIGN-N80Q, were created using a QuickChange XL site-directed mutagenesis kit (Stratagene, La Jolla, CA), pEGFP-C1/DC-SIGN and pEGFP-N1/GFP-DC-SIGN as the templates, respectively, and the following mutagenic primers (the mutation site is indicated in *italics*): 5'-GACGCGATCTACCAG*CAG*CTGACCCAGCTTAAAG (primer C) and 5'-CTTTAAGCTGGGTCAG*CTG*CTGGTAGATCGCGTC (primer D). The two tandem repeat deletion constructs, DC-SIGN-ΔRepeats and GFP-DC-SIGN-ΔRepeats, were made by using an overlap extension PCR strategy. To generate DC-SIGN-ΔRepeats, a 0.3 kb fragment encoding the N-terminal residues 1–80 of DC-SIGN was amplified by PCR with pEGFP-C1/DC-SIGN as the template and the following two primers: 5'-CCACCGGTCGCCACCATGAGTGACTCCAAGGAACCA (primer E) and 5'-*CCATTCCCAGGGACAGGGGTGGCAGTTCTGGTA*GATCGCGTCTTGCCTG (primer F), in which Primer E encodes an *Age*I site (underlined) and primer F contains the overlap extension sequence (in *italics*). A 0.5 kb fragment encoding the C-terminal residues 253–404 of DC-SIGN was amplified by PCR with the following two primers: 5'-*TACCAGAACTGCCACCCCTGTCCCTGGGAATGG* (primer G) and primer B, in which the overlap extension sequence is indicated in *italics* in primer G, and primer B encodes a *Not*I site (underlined). The two PCR products were then purified and mixed as the templates for the second round overlap extension PCR using primers E and B and the resulting product was digested and inserted into the pEGFP-N1 vector through the *Age*I and *Not*I sites. GFP-DC-SIGN-ΔRepeats was generated in a similar manner, using pEGFP-N1/GFP-DC-SIGN as the template: the first PCR used primer H 5'-CGGGATCCCGCCACCATGGTGAGCAAGGGC (*BamH*I site is underlined) and primer F to generate a 1 kb fragment encoding the EGFP gene and residues 1–80 of DC-SIGN; and primers G and B were used to generate the 0.5 kb fragment encoding the C-terminal peptide of DC-SIGN. The 1 kb and 0.5 kb fragments were then mixed as the templates for the second round overlap extension PCR with primers H and B and the resulting product was digested and cloned into the pEGFP-N1 vector through *BamH*I and *Not*I sites. As most antibodies against DC-SIGN recognize its CRD, an AU1 tag was introduced at the C-terminus of the DC-SIGN-ΔCRD construct: 5'-AAGCGGCCGCTTTA*TATGTATCTGTAGGTGTC*CAGGCGTTCCACTGCAGC (primer I). Primer I encodes a *Not*I site (underlined) and the AU1 tag (in *italics*), and the DC-SIGN-ΔCRD was generated by PCR using primer E and primer I with pEGFP-C1/DC-SIGN as the template. The amplified fragment was then digested with *Age*I and *Not*I, and cloned into the pEGFP-N1 vector, from which the FP gene was removed by digesting with *Age*I and *Not*I. Similarly, primer H and primer J, 5'-TTTTGGTTTTGCGGCCGCTTTACAGGCGTTCCACTGCAGC, (*Not*I site is underlined) were employed to generate the GFP-DC-SIGN-ΔCRD fragment by PCR with pEGFP-N1/GFP-DC-SIGN as the template and the resulting product was digested and cloned into pEGFP-N1 through the *BamH*I and *Not*I sites. Construction of GFP-DC-SIGN-Δ37 was carried out through an overlap extension PCR strategy. The 0.7 kb EGFP gene was amplified by PCR with pEGFP-N1 (Clontech) as the template and primer H and the following primer: 5'-*CACCAGGGGACCATGGCCAAGCTTGTACAGCTC*GTCCATGCCGAG (primer K).

Primer H contains a *BamH*I site and primer K contains the overlap extension sequence (in *italics*). The 1.1 kb fragment encoding residues 38–404 of DC-SIGN was amplified by PCR using pEGFP-C1/DC-SIGN as the template and the following two primers: 5'-*GAGCTGTACAAGCTTGGCCATGGTCCCCTGGTG* (primer L) and primer B. Primer L contains the overlap extension sequence (in *italics*) and primer B contains a *Not*I site. The two PCR products were purified and mixed as templates for the second overlap extension PCR, using primer H and primer B. The resulting product was digested and inserted into the pEGFP-N1 vector through the *BamH*I and *Not*I sites.

All of the constructs described above were confirmed by DNA sequencing. A schematic drawing of the constructs is shown in Figure 1 A.

Cell culture and transfection

NIH3T3 cells were maintained in Dulbecco's modified Eagle's medium (DMEM) (Invitrogen) supplemented with 10% fetal bovine serum (FBS), 50 U/ml penicillin G and 50 μg/ml streptomycin at 37°C in 5% (v/v) CO_2. For observation under the microscope, cells were seeded in 35 mm glass-bottom MatTek dishes (MatTek Corp., Ashland, MA) at 10^5 cells/dish one day before transfection. Plasmids were introduced into the cells by following standard protocols employing either Fugene 6 (Roche, Indianapolis, IN) or Lipofectamine (Invitrogen) at 2 μg cDNA/dish. After transfection, cells were maintained in normal growth medium for at least two days either in a 37°C incubator (for the expression of wt DC-SIGN) or in a 32°C incubator (for the expression of DC-SIGN mutant forms) with 5% CO_2. Incubation at 32°C facilitates protein folding and hence plasma membrane translocation, as reported previously (11, 35). For immunoblotting of DC-SIGN and mutant proteins, samples were prepared using a similar procedure as above except that the cells were plated in 60 mm petri dishes and transfected at 6 μg cDNA/dish.

Immunoblotting

After cultivating the transfected cells for two days, the cells were washed with ice-cold phosphate buffered saline (PBS) and solubilized with Laemmli sample buffer (200 μl). The lysates were then heat denatured for 10 min at 95 °C, and stored at −80 °C until use. Samples were electrophoretically separated with a 4–12% Bis-Tris gel (Invitrogen), and blotted onto a Hybond-P membrane (Amersham Biosciences, Little Chalfont, UK). After blocking the membrane with 5% skim milk in Tris Buffered Saline-Tween 20 (TBS-T) buffer, wt DC-SIGN and the mutant proteins were stained with three types of antibodies: DCN46 (BD Biosciences, San Jose, CA), for the detection of wt DC-SIGN, GFP-DC-SIGN, DC-SIGN-Δ37, GFP-DC-SIGN-Δ37, DC-SIGN-N80Q and GFP-DC-SIGN-N80Q; 120507 (R&D Systems, Minneapolis, MN), for the detection of DC-SIGN-ΔRepeats and GFP-DC-SIGN-ΔRepeats; H-200 (Santa Cruz Biotechnology, Santa Cruz, CA), for the detection of DC-SIGN-ΔCRD and GFP-DC-SIGN-ΔCRD, respectively. After washing, the membranes were incubated with either goat anti-mouse AlexaFluor 680-conjugated IgG (Invitrogen; for DCN46 and 120507 primary Ab) or goat anti-rabbit AlexaFluor 680-conjugated IgG (Invitrogen; for H-200 primary Ab). The proteins were visualized by scanning the membranes on an Odyssey infrared imaging system (LI-COR Biosciences, Lincoln, Nebraska).

Fluorescence labeling

At the time of observation, cells expressing GFP fusions were washed thoroughly with PBS and then incubated with Hank's balanced salt solution (HBSS) lacking phenol red during measurements on the microscope. For cells expressing DC-SIGN and its mutant forms without the EGFP tag, mAb were employed to stain the receptors on cell surfaces. Commercially obtained antibodies include the following: mouse monoclonal IgG2b specific

for human DC-SIGN (DCN46; BD Biosciences); mouse monoclonal IgG2a AU1 antibody FITC conjugate (FITC-130L; Covance Inc., Princeton, NJ); mouse monoclonal IgG2b against human DC-SIGN (120507; R&D Systems); AlexaFluor 488-conjugated goat polyclonal IgG specific for mouse IgG (Invitrogen). For some measurements, the 120507 mAb was directly conjugated to AlexaFluor488, by using a slightly modified procedure to that based on the kit and the protocol from Invitrogen (mp10235). In our experience, a 5:1 molar ratio of AlexaFluor 488 to antibody usually results in a mean labeling ratio of ~ 1 dye molecule per IgG. To increase the final dye/antibody ratio, we aimed for a labeling ratio of 3 dyes: 1 IgG. After labeling, the mean dye to IgG ratio was estimated to be 3–7 based on the corrected absorbance of proteins at 280 nm (major peak of proteins and tails of AlexaFluor 488 spectrum) and at 494 nm (AlexaFluor 488 fluorophores only). The manner in which these reagents were employed to facilitate confocal imaging and FRAP measurements is detailed in Supplemental Table S1 (Table S1, Supporting Information).

Microscopy

Cell imaging and FRAP measurements were carried out on an inverted laser scanning confocal microscope FV1000 (Olympus) with an oil immersion objective (60×, N.A. 1.42; Olympus) at 37°C. For cell imaging, an excitation wavelength of 488 nm (argon laser) at 6% power was used and fluorescence emission was collected at 500–540 nm. For each cell image 1024×1024 pixels were probed at 2 μs/pixel with a pixel size of 69 nm, except that for the FITC-130L mAb labeled cells the images were collected at 10 μs/pixel due to the relatively low brightness of fluorescein. For cells expressing the GFP-tagged DC-SIGN and mutant constructs, some intracellular fluorescence was observed during imaging, likely due to the ongoing protein synthesis and delivery. To minimize the effect of intracellular fluorescence in our imaging and domain size analyses, we chose cells in which the majority of fluorescence was on the membrane, and minimal intracellular fluorescence was observed. This was achieved in part by imaging cells at later stages after transfection, i.e. 48–72 hours after transfection, when the majority of the GFP-fusion proteins had been translocated to the plasma membrane and there was minimal remaining synthesis due to the degradation of the transiently transfected plasmids. Further, 2D confocal image slices were chosen for analysis by identifying z-positions where the distribution of fluorescence was either on the dorsal or ventral cell surfaces (such that no nuclear exclusion of fluorescence was observed), or confined to the cell periphery (where the fluorescence is visible as punctate outline on the plasma membrane) (See also Supplemental Figure S5).

For FRAP measurements, a 64×64 pixel (0.11 μm/pixel) area was continuously scanned by using the 488 nm laser at 6% power for 100–500 frames at 2 μs/pixel rate (except that FITC-130L labeled cells were imaged at 10 μs/pixel), and photobleaching was carried out simultaneously at the third frame by using the SIM scanner with the 405 nm diode laser. For cells expressing GFP fusions or labeled with FITC-130L mAb, the 405 nm laser line was used at 50% power, and for cells labeled with AlexaFluor 488-conjugated mAb the power was set at 100% as the Alexa fluorophores are relatively brighter and more stable. For all sample sets the photobleaching time was 43 ms with the tornado scan feature, and the effective bleached area ranged from 1.4 to 2 μm in diameter. For the FRAP studies on the GFP wt DC-SIGN and the GFP mutant forms, the contribution of the GFP fusions in the internal biosynthetic and endocytotic pathways was minimized by selecting cells in which the intracellular background was small compared to the fluorescence of the microdomains. It is possible that the small amount of recovery measured in Figure 3 B, for example, was due to a small amount of fusion protein in internal membrane compartments where it was laterally mobile (See also Supplemental Figure S5).

Data analysis

The size of the microdomains on the cell surface, formed by wt DC-SIGN as well as the cytoplasmic tail truncation and N-linked glycosylation site mutants, was estimated by analyzing images from cell samples using an automated program called Localizer (36) written in Igor Pro (WaveMetrics, Inc., Oregon) software. The fluorescent microdomains on cell images, called “emitters” in the Localizer program, were segmented by a generalized likelihood ratio test (GLRT) algorithm (37), which is specifically designed to detect PSF-shaped (i.e., Gaussian-like) spots. Tentative emission microdomains were passed into localization routines, in which a symmetric Gaussian was fit to every microdomain using Levenberg-Marquardt least-squares minimization. Localizations that were too close together to be independent were discarded. The standard deviation (σ, pixel) was obtained from the fitting as the width of the “emitter”. The size (diameter, nm) of the microdomains was then calculated by using the following equation: FWHM = σ pixel × 2.3 × 69 nm/pixel.

The FRAP data analysis has been described previously (7). Briefly, after subtracting background and correcting for the photobleaching effects during pre-bleach and post-bleach observation, the % recovery was calculated as: $P(t) = 100 \times [F(t) - F(0)]/[F(-) - F(0)]$, where $F(-)$ is the mean pre-bleach fluorescence intensity and $F(0)$ is the mean fluorescence intensity right after bleaching. The function $P(t)$ was then fit to an expression, $P(t) = P_\infty \times [t/(t+\tau_D)]$, with P_∞ and τ_D as free parameters, using Igor Pro 6.0 (Wavemetrics, Portland, OR). From the fit, the values of P_∞ were taken as mobile percentages. The values of τ_D were used to calculate the diffusion coefficient D using the equation: $D = \langle\omega^2\rangle /[4\ \tau_D]$, where ω is the radius of the bleached area.

Supplementary Material

Refer to Web version on PubMed Central for supplementary material.

Acknowledgments

We thank Drs. Ilya Levental and Kai Simmons at Max Planck Institute for Molecular Cell Biology and Genetics (Germany) for carrying out the GPMV experiments and helpful discussion; Dr. Peter Dedecker at the University of Leuven (Belgium) for providing the Igor plug-in for microdomain size analysis and helpful discussion; and Dr. Dan Littman, New York University and Howard Hughes Medical Institute, New York, for providing the pMX/GFP-DC-SIGN construct. This work was supported primarily by NIH grant GM-041402 (K.J. and N.L.T.) and also by the NIH Cell Migration Consortium NIH GM 64346 (K.J.) and NSF grant MCB-0641087 (N.L.T).

References

1. Geijtenbeek TB, den Dunnen J, Gringhuis SI. Pathogen recognition by DC-SIGN shapes adaptive immunity. Future Microbiol. 2009; 4:879–890. [PubMed: 19722841]
2. Snyder GA, Ford J, Torabi-Parizi P, Arthos JA, Schuck P, Colonna M, Sun PD. Characterization of DC-SIGN/R Interaction with Human Immunodeficiency Virus Type 1 gp120 and ICAM Molecules Favors the Receptor's Role as an Antigen-Capturing Rather than an Adhesion Receptor. J Virol. 2005; 79:4589–4598. [PubMed: 15795245]
3. Cambi A, de Lange F, van Maarseveen NM, Nijhuis M, Joosten B, van Dijk EMHP, de Bakker BrI, Fransen JAM, Bovee-Geurts PHM, van Leeuwen FN, Van Hulst NF, Figdor CG. Microdomains of the C-type lectin DC-SIGN are portals for virus entry into dendritic cells. J Cell Biol. 2004; 164:145–155. [PubMed: 14709546]
4. Koopman M, Cambi A, de Bakker BI, Joosten B, Figdor CG, van Hulst NF, Garcia-Parajo MF. Near-field scanning optical microscopy in liquid for high resolution single molecule detection on dendritic cells. FEBS Lett. 2004; 573:6–10. [PubMed: 15327966]
5. Neumann AK, Thompson NL, Jacobson K. Distribution and lateral mobility of DC-SIGN on immature dendritic cells–implications for pathogen uptake. J of Cell Sci. 2008; 121:634–643. [PubMed: 18270264]

6. Cambi A, Koopman M, Figdor CG. How C-type lectins detect pathogens. Cell Microbiol. 2005; 7(4):481–488. [PubMed: 15760448]
7. Itano Michelle S, Neumann Aaron K, Liu P, Zhang F, Gratton E, Parak Wolfgang J, Thompson Nancy L, Jacobson K. DC-SIGN and Influenza Hemagglutinin Dynamics in Plasma Membrane Microdomains Are Markedly Different. Biophys J. 2011; 100:2662–2670. [PubMed: 21641311]
8. Zuckerman DM, Hicks SW, Charron G, Hang HC, Machamer CE. Differential regulation of two palmitoylation sites in the cytoplasmic tail of the beta1-adrenergic receptor. J Biol Chem. 2011; 286:19014–19023. [PubMed: 21464135]
9. Chapple JP, Hardcastle AJ, Grayson C, Willison KR, Cheetham ME. Delineation of the Plasma Membrane Targeting Domain of the X-Linked Retinitis Pigmentosa Protein RP2. Invest Ophthalmol & Vis Sci. 2002; 43:2015–2020. [PubMed: 12037013]
10. Webb Y, Hermida-Matsumoto L, Resh MD. Inhibition of Protein Palmitoylation, Raft Localization, and T Cell Signaling by 2-Bromopalmitate and Polyunsaturated Fatty Acids. J Bio Chem. 2000; 275:261–270. [PubMed: 10617614]
11. Liu P, Sudhaharan T, Koh RM, Hwang LC, Ahmed S, Maruyama IN, Wohland T. Investigation of the dimerization of proteins from the epidermal growth factor receptor family by single-wavelength fluorescence cross-correlation spectroscopy. Biophys J. 2007; 93:684–698. [PubMed: 17468161]
12. Caparrós E, Munoz P, Sierra-Filardi E, Serrano-Gómez D, Puig-Kröger A, Rodríguez-Fernández JL, Mellado M, Sancho J, Zubiaur M, Corbí AL. DC-SIGN ligation on dendritic cells results in ERK and PI3K activation and modulates cytokine production. Blood. 2006; 107:3950–3958. [PubMed: 16434485]
13. Curtis BM, Scharnowske S, Watson AJ. Sequence and expression of a membrane-associated C-type lectin that exhibits CD4-independent binding of human immunodeficiency virus envelope glycoprotein gp120. Proc Natl Acad Sci USA. 1992; 89:8356–8360. [PubMed: 1518869]
14. Vasta GR. Roles of galectins in infection. Nat Rev Micro. 2009; 7:424–438.
15. Serrano-Gómez D, Sierra-Filardi E, Martínez-Nuñez RT, Caparrós E, Delgado R, Muñoz-Fernández MA, Abad MA, Jimenez-Barbero J, Leal M, Corbí AL. Structural Requirements for Multimerization of the Pathogen Receptor Dendritic Cell-specific ICAM3-grabbing Non-integrin (CD209) on the Cell Surface. J Biol Chem. 2008; 283:3889–3903. [PubMed: 18073208]
16. Sprague BL, McNally JG. FRAP analysis of binding: proper and fitting. Trends Cell Biol. 2005; 15:84–91. [PubMed: 15695095]
17. Lippincott-Schwartz J, Snapp E, Kenworthy A. Studying protein dynamics in living cells. Nat Rev Mol Cell Biol. 2001; 2:444–456. [PubMed: 11389468]
18. Baumgart T, Hammond AT, Sengupta P, Hess ST, Holowka DA, Baird BA, Webb WW. Large-scale fluid/fluid phase separation of proteins and lipids in giant plasma membrane vesicles. Proc Natl Acad Sci USA. 2007; 104:3165–3170. [PubMed: 17360623]
19. Keller H, Lorizate M, Schwille P. PI(4,5)P2 Degradation Promotes the Formation of Cytoskeleton-Free Model Membrane Systems. Chemphyschem. 2009; 10(16):2805–2812. [PubMed: 19784973]
20. Gringhuis SI, den Dunnen J, Litjens M, van der Vlist M, Geijtenbeek TBH. Carbohydrate-specific signaling through the DC-SIGN signalosome tailors immunity to Mycobacterium tuberculosis, HIV-1 and Helicobacter pylori. Nat Immunol. 2009; 10:1081–1088. [PubMed: 19718030]
21. Hodges A, Sharrocks K, Edelmann M, Baban D, Moris A, Schwartz O, Drakesmith H, Davies K, Kessler B, McMichael A, Simmons A. Activation of the lectin DC-SIGN induces an immature dendritic cell phenotype triggering Rho-GTPase activity required for HIV-1 replication. Nat Immunol. 2007; 8:569–577. [PubMed: 17496896]
22. Feinberg H, Guo Y, Mitchell DA, Drickamer K, Weis WI. Extended Neck Regions Stabilize Tetramers of the Receptors DC-SIGN and DC-SIGNR. J Biol Chem. 2005; 280:1327–1335. [PubMed: 15509576]
23. Yu QD, Oldring AP, Powlesland AS, Tso CKW, Yang C, Drickamer K, Taylor ME. Autonomous Tetramerization Domains in the Glycan-binding Receptors DC-SIGN and DC-SIGNR. J Mol Biol. 2009; 387:1075–1080. [PubMed: 19249311]
24. Horejsi V, Zhang W, Schraven B. Transmembrane adaptor proteins: organizers of immunoreceptor signalling. Nat Rev Immunol. 2004; 4:603–616. [PubMed: 15286727]

25. Rapraeger AC. Syndecan-Regulated Receptor Signaling. J Cell Biol. 2000; 149:995–998. [PubMed: 10831602]
26. Avota E, Gulbins E, Schneider-Schaulies S. DC-SIGN mediated sphingomyelinase-activation and ceramide generation is essential for enhancement of viral uptake in dendritic cells. PLoS Pathog. 2011; 7 e1001290.
27. Gumbiner BM. Regulation of cadherin-mediated adhesion in morphogenesis. Nat Rev Mol Cell Biol. 2005; 6:622–634. [PubMed: 16025097]
28. Sanes JR. The Basement Membrane/Basal Lamina of Skeletal Muscle. J Biol Chem. 2003; 278:12601–12604. [PubMed: 12556454]
29. Dubash AD, Menold MM, Samson T, Boulter E, García-Mata R, Doughman R, Burridge K. Chapter 1 Focal Adhesions: New Angles on an Old Structure. Int Rev Cell Mol Biol. 2009; 277:1–65. [PubMed: 19766966]
30. Burridge K, Fath K, Kelly T, Nuckolls G, Turner C. Focal Adhesions: Transmembrane Junctions Between the Extracellular Matrix and the Cytoskeleton. Annu Rev Cell Biol. 1988; 4:487–525. [PubMed: 3058164]
31. Geiger B, Bershadsky A, Pankov R, Yamada KM. Transmembrane crosstalk between the extracellular matrix and the cytoskeleton. Nat Rev Mol Cell Biol. 2001; 2:793–805. [PubMed: 11715046]
32. O'Reilly MK, Paulson JC. Siglecs as targets for therapy in immune-cell-mediated disease. Trends Pharmacol Sci. 2009; 30:240–248. [PubMed: 19359050]
33. Crocker PR, Paulson JC, Varki A. Siglecs and their roles in the immune system. Nat Rev Immunol. 2007; 7:255–266. [PubMed: 17380156]
34. Guo Y, Feinberg H, Conroy E, Mitchell DA, Alvarez R, Blixt O, Taylor ME, Weis WI, Drickamer K. Structural basis for distinct ligand-binding and targeting properties of the receptors DC-SIGN and DC-SIGNR. Nat Struct Mol Biol. 2004; 11:591–598. [PubMed: 15195147]
35. Pohlmann S, Baribaud F, Lee B, Leslie GJ, Sanchez MD, Hiebenthal-Millow K, Munch J, Kirchhoff F, Doms RW. DC-SIGN interactions with human immunodeficiency virus type 1 and 2 and simian immunodeficiency virus. J Virol. 2001; 75:4664–4672. [PubMed: 11312337]
36. http://www.igorexchange.com/project/Localizer.
37. Serge A, Bertaux N, Rigneault H, Marguet D. Dynamic multiple-target tracing to probe spatiotemporal cartography of cell membranes. Nat Meth. 2008; 5:687–694.

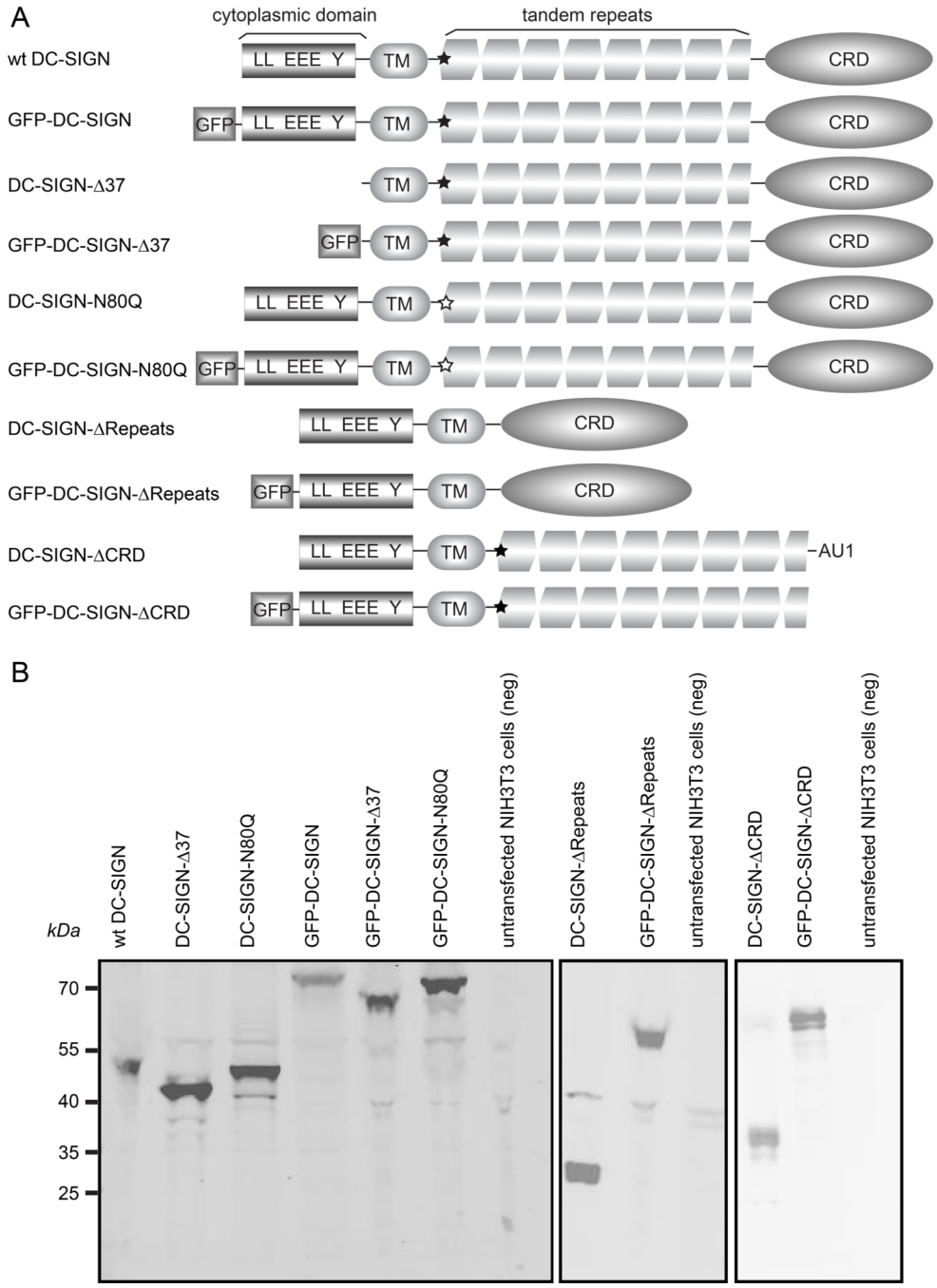

Figure 1. Construction and expression of DC-SIGN and its mutant forms

A) Schematic overview of DC-SIGN constructs. LL, di-leucine motif; EEE, tri-acidic cluster; Y, a tyrosine-based activation motif; TM, transmembrane region; CRD, carbohydrate recognition domain. Solid star (black) denotes Asn^{80} glycosylation site. Open star (white) denotes Asn^{80} changed to a Gln^{80}. B) Detection of DC-SIGN and its mutant forms by Western blot. Cell lysates from NIH3T3 cells transiently transfected with the indicated constructs were resolved by SDS-PAGE and subjected to Western blot analysis using DCN46 mAb (left panel), 120507 mAb (middle panel) and H-200 polyclonal Ab (right panel), respectively. Lysates from untransfected NIH3T3 cells were used as negative controls in each panel.

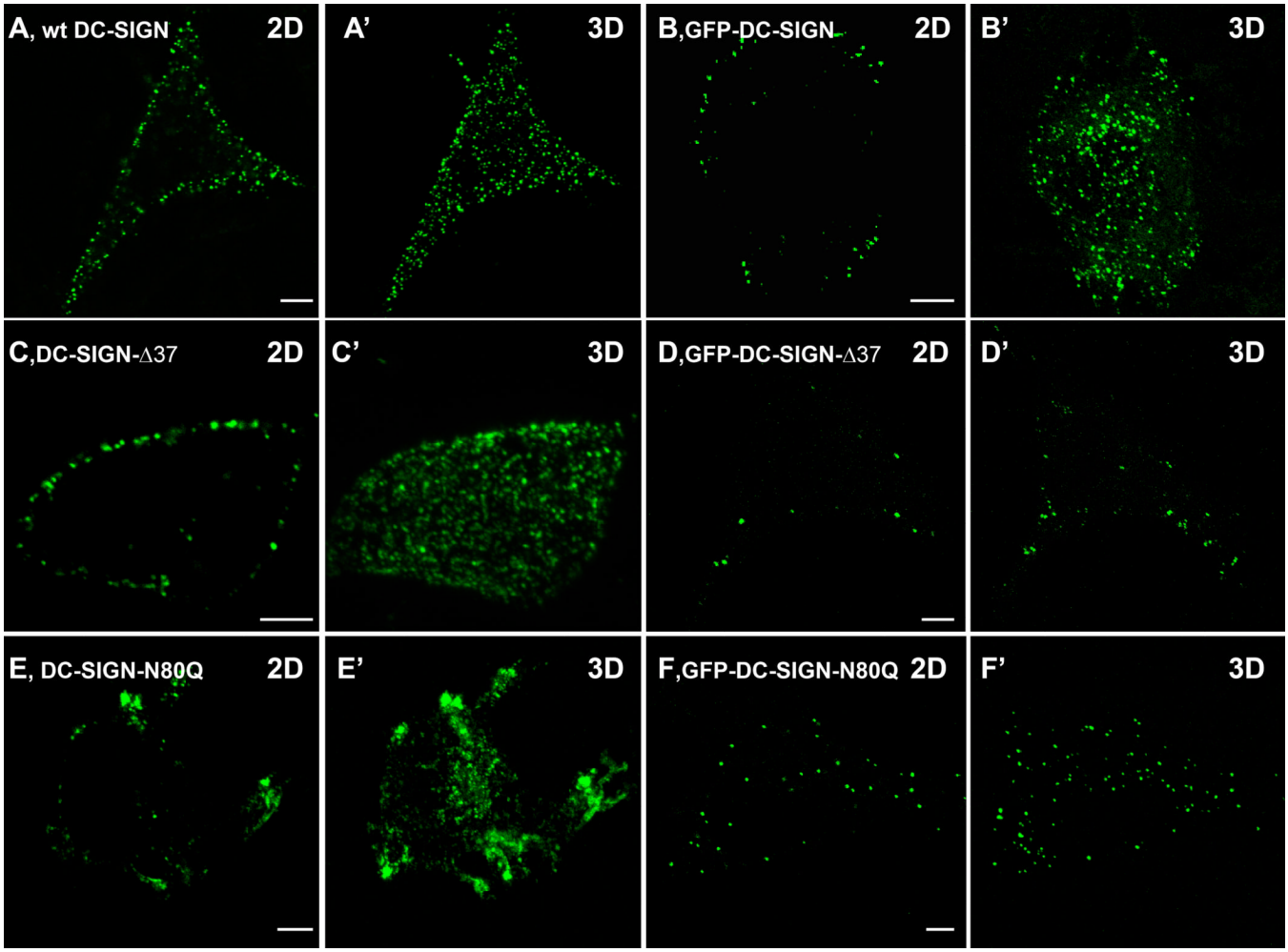

Figure 2. Wt DC-SIGN, cytoplasmic truncation and glycosylation site mutation of DC-SIGN form discrete and stable microdomains on cell surfaces

Confocal images of NIH3T3 cells expressing wt DC-SIGN (A and A'), GFP-DC-SIGN (B and B'), DC-SIGN-Δ37 (C and C'), GFP-DC-SIGN-Δ37 (D and D'), DC-SIGN-N80Q (E and E') and GFP-DC-SIGN-N80Q (F and F'). '2D' represents a single two-dimensional confocal slice and '3D' represents a three-dimensional maximum intensity projection of images from confocal z-stacks. Note that for non-GFP tagged constructs, antibody staining was carried out on non-permeabilized cells so that the staining was confined to the plasma membrane. Bars, 5 μm.

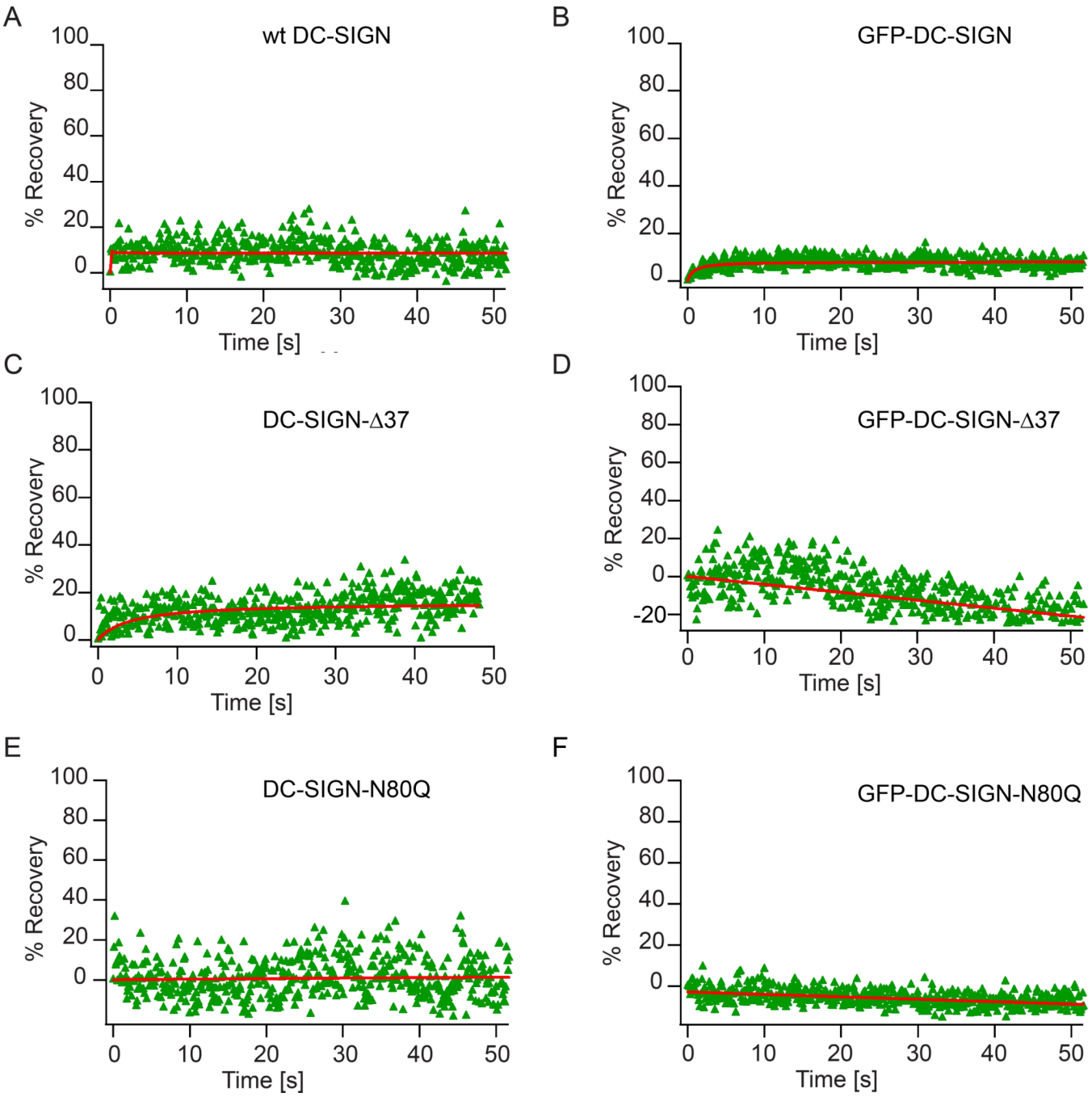

Figure 3. DC-SIGN, DC-SIGN-Δ37 and DC-SIGN-N80Q within microdomains do not appreciably exchange with molecules of the same type in the surrounding environment

(A–F) Normalized fluorescence recovery of a small region containing a bleached microdomain on NIH3T3 cells expressing wt DC-SIGN (A), GFP-DC-SIGN (B), DC-SIGN-Δ37 (C), GFP-DC-SIGN-Δ37 (D), DC-SIGN-N80Q (E) and GFP-DC-SIGN-N80Q (F). Graphs A–C were fit to equation $P(t) = P_{\infty} \times [t/(t+\tau_D)]$, while graphs D–F could not be fit to the equation, so a linear fitting equation, $P(t) = a + bt$, with a and b as free parameter constants, was applied instead. The red lines on each graph indicate the results from fitting to the appropriate equations.

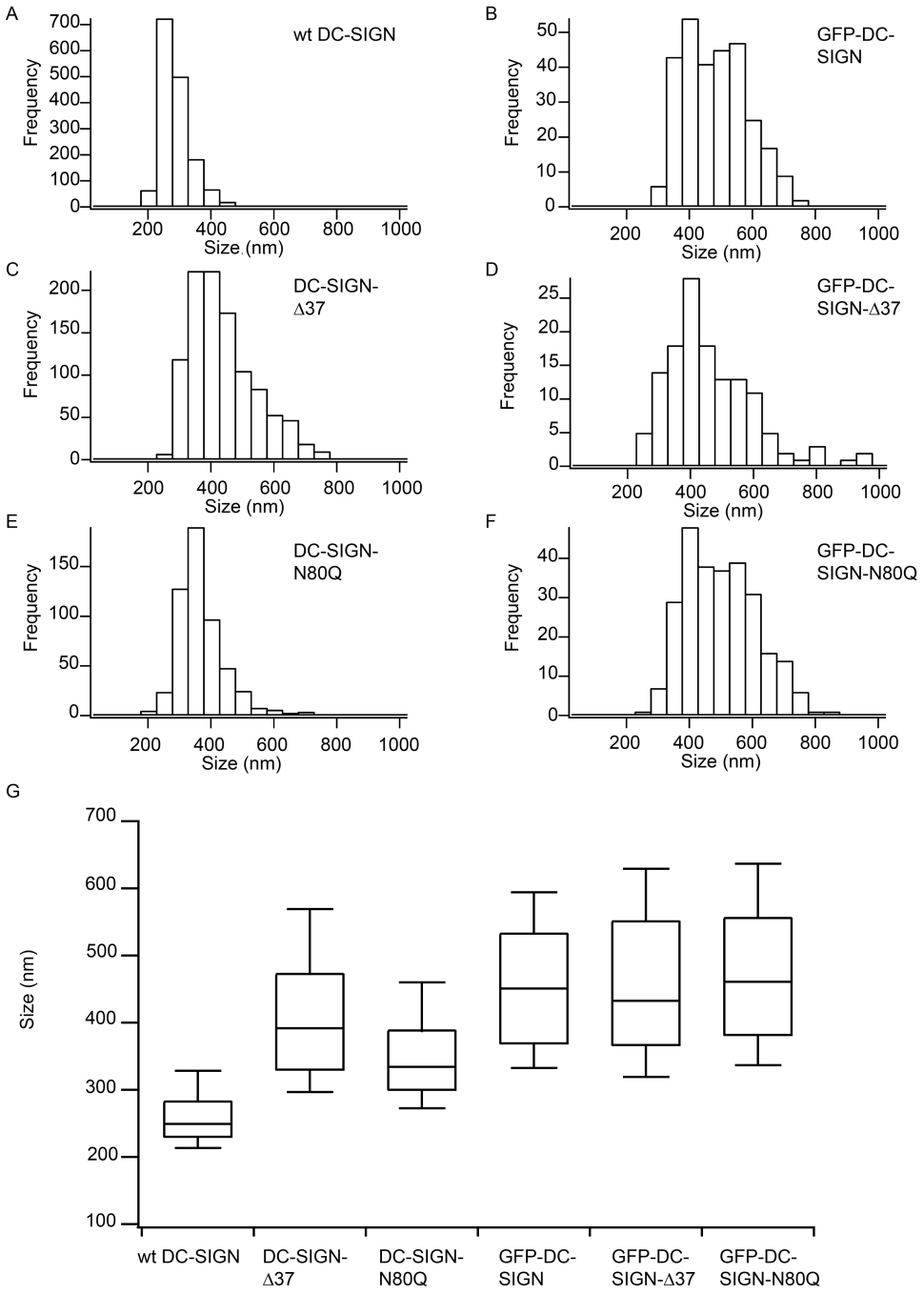

Figure 4. Size distribution of microdomains formed by DC-SIGN and its mutant forms

(A–F) Microdomain size distribution of wt DC-SIGN (A), GFP-DC-SIGN (B), DC-SIGN-Δ37 (C), GFP-DC-SIGN-Δ37 (D), DC-SIGN-N80Q (E), and GFP-DC-SIGN-N80Q (F). (G), Box and whisker plot describing the size distributions for DC-SIGN and mutant microdomains where the midline within the box represents the median of the distribution, the top and bottom of the box represents the 75th and 25th percentile of the distribution, respectively, and the top and bottom tips of the whisker represent the 90th and 10th percentile, respectively. The size distributions were measured from single confocal image slices near the ventral surfaces of the cells.

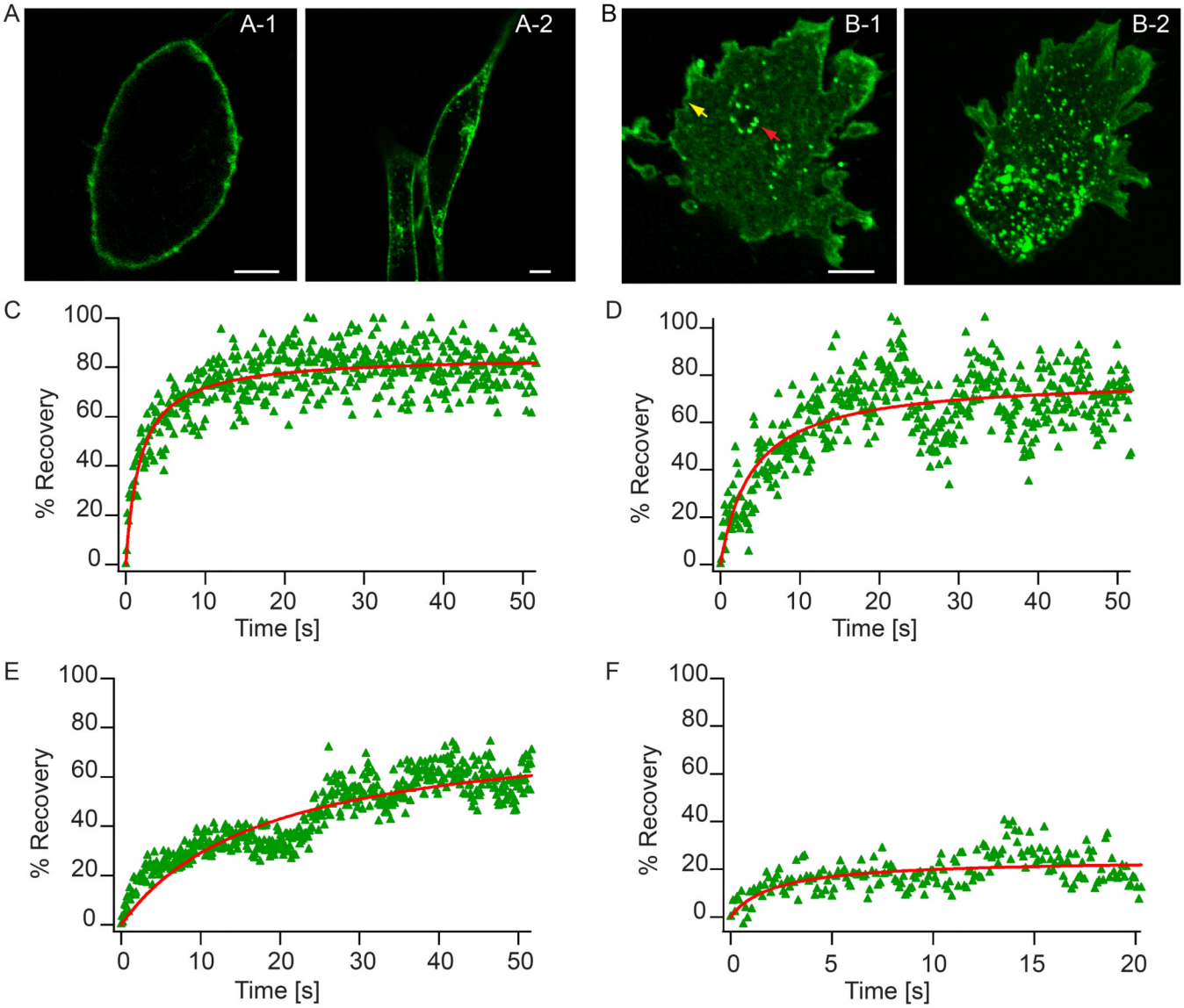

Figure 5. The tandem repeats deletion mutant of DC-SIGN exhibits both free membrane diffusion and dynamic microdomains on cell surfaces

(A) Confocal slice of NIH3T3 cells expressing GFP-DC-SIGN-Δrepeats (A-1) or DC-SIGN-Δrepeats labeled by AlexaFluor 488-conjugated 120507 mAb (A-2); both at lower expression levels. (B) A sample image, at higher expression levels, of a cell expressing GFP-DC-SIGN-Δrepeats which exhibits both dynamic microdomains and diffuse membrane fluorescence. (B-1), Confocal image of a ventral surface section; dynamic microdomains are indicated by a red arrow and the diffuse membrane fluorescence is indicated by a yellow arrow. (B-2), maximum intensity projection from confocal z-stacks of another cell. (C) and (D), Representative FRAP curves measured on the diffusive membrane areas of NIH3T3 cells expressing GFP-DC-SIGN-ΔRepeats (C) or DC-SIGN-ΔRepeats (AlexaFluor 488 conjugated 120507 mAb label) (D), respectively (both at lower expression levels). (E) and (F), Representative FRAP curves measured on the 'dynamic microdomain' areas of NIH3T3 cells expressing GFP-DC-SIGN-ΔRepeats (E) or DC-SIGN-ΔRepeats (AlexaFluor 488 conjugated 120507 mAb label) (F), respectively. Bars, 5 μm.

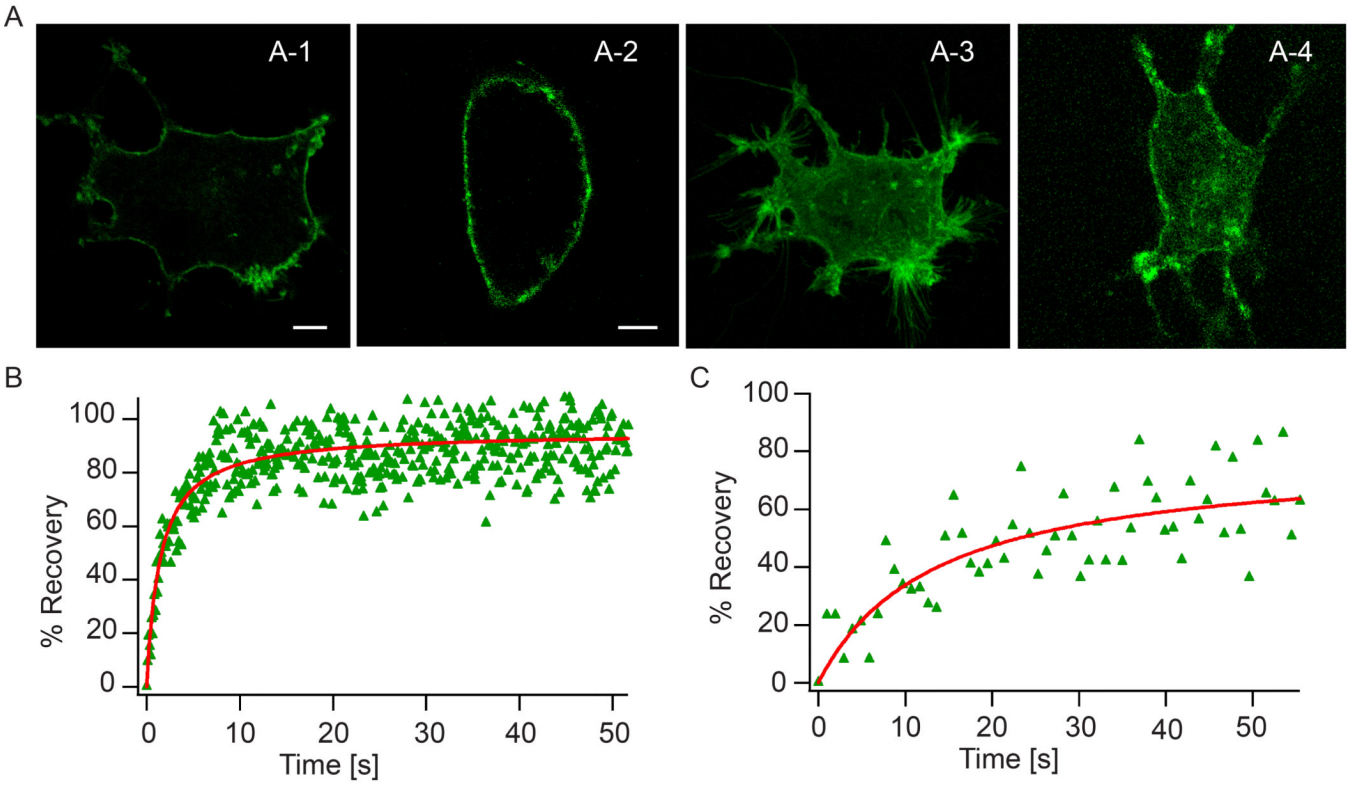

Figure 6. Removal of the CRD results in a complete loss of microdomain formation on the cell surface

(A, from *left* to *right*), 2D confocal images of cells expressing GFP-DC-SIGN-ΔCRD (A-1) and DC-SIGN-ΔCRD labeled by anti-AU1 FITC conjugated mAb (FITC-130L, A-2); Maximum intensity projections from confocal z-stacks of cells expressing GFP-DC-SIGN-ΔCRD (A-3) and DC-SIGN-ΔCRD labeled by FITC-130L mAb (A-4); (B–C), representative FRAP curves on cells expressing GFP-DC-SIGN-ΔCRD (B) and DC-SIGN-ΔCRD labeled by FITC-130L mAb (C). Bars, 5 μm.

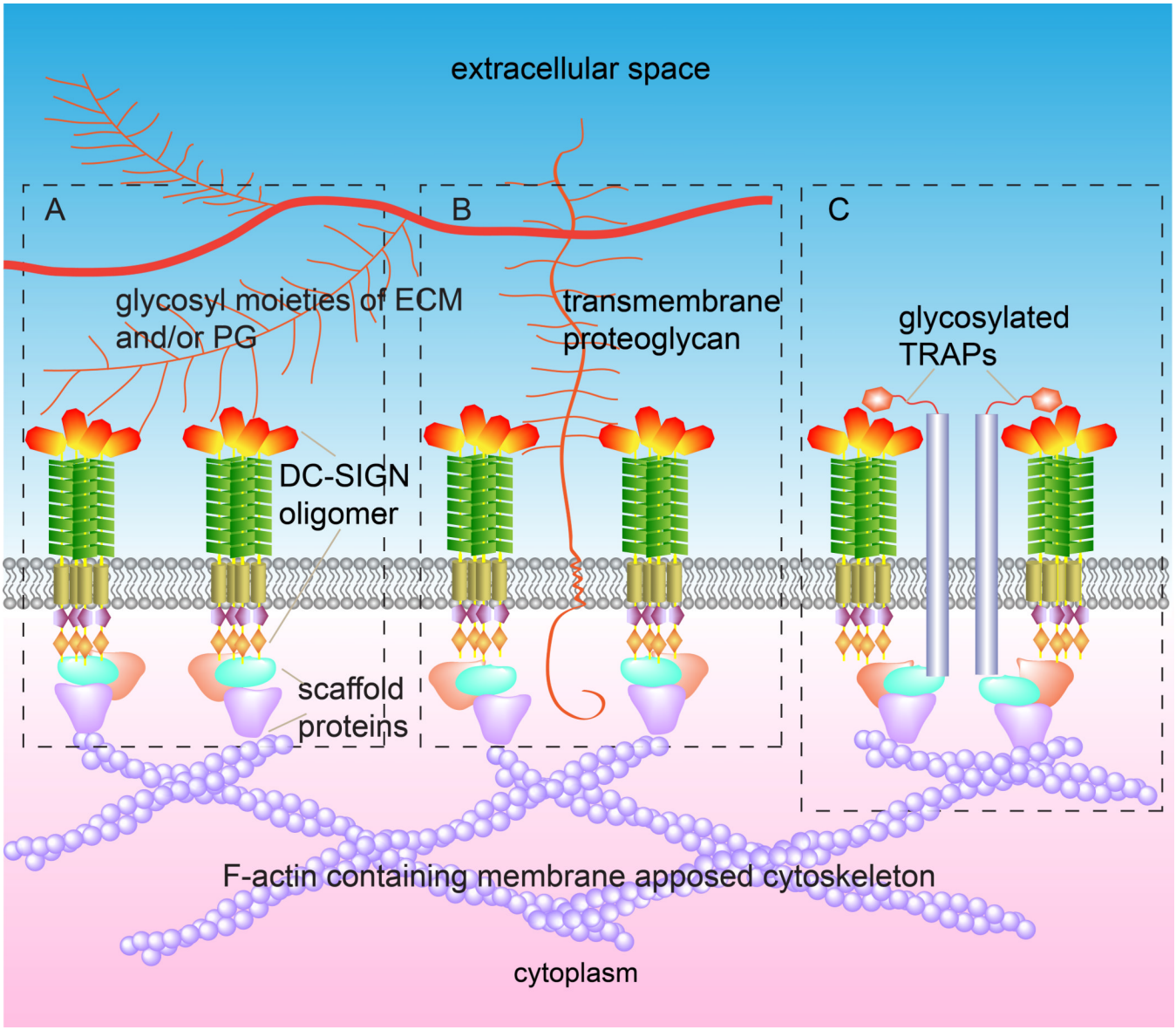

Figure 7. Models for DC-SIGN microdomain formation and stability

(A–B) Microdomain formation could be primarily facilitated and stabilized through interactions between CRDs of DC-SIGN and ECM components. Several possible ways of linking the CRD to the ECM can be envisioned: first, the CRD binds directly to glycosaminoglycans and/or proteoglycans or glycosyl moieties of proteins in the ECM (A) or, second, CRD may bind to transmembrane proteoglycans which could cross-link the receptor to the ECM as well as to the cytoskeleton (B). On the other hand, glycosylated transmembrane adaptor proteins (TRAPs) may have *cis* interactions with DC-SIGN, and thereby link the receptor to the cytoskeleton, albeit indirectly. Such proteins may serve as co-receptors with DC-SIGN serving to distinguish different pathogens and to differentiate downstream signaling pathways. ECM, extracellular matrix. PG, proteoglycan. TRAPs, transmembrane adaptor proteins.

Table 1

Characteristics of DC-SIGN and its mutant forms on the cell surface

Construct	Forms surface microdomains	Microdomain size (nm: +/− SD, sample size N)	Recovery after photobleaching	Recovery percentage (% : +/− SEM)	Diffusion coefficient ($\mu m^2/s$: +/− SEM)
wt DC-SIGN	Yes	262 +/− 49 N = 1568	No	_	_
GFP-DC-SIGN	Yes	457 +/− 101 N = 289	No	_	_
DC-SIGN-Δ37	Yes	411 +/− 106 N = 1064	No	_	_
GFP-DC-SIGN-Δ37	Yes	465 +/− 140 N = 134	No	_	_
DC-SIGN-N80Q	Yes	355 +/− 84 N = 582	No	_	_
GFP-DC-SIGN-N80Q	Yes	473 +/− 114 N = 268	No	_	_
DC-SIGN-Δrepeats	Partially	_	Yes	67 +/− 10 (N = 10)	0.08 +/− 0.03 (N = 10)
GFP-DC-SIGN-Δrepeats	Partially	_	Yes	78 +/− 5 (N = 13)	0.12 +/− 0.02 (N = 13)
DC-SIGN-ΔCRD	No	_	Yes	73 +/− 7 (N= 11)	0.02 +/− 0.01 (N = 11)
GFP-DC-SIGN-ΔCRD	No	_	Yes	95 +/− 4 (N = 15)	0.18 +/− 0.02 (N = 15)